Journal of Energy Storage 32 (2020) 101798

Contents lists available at ScienceDirect

Journal of Energy Storage

journal homepage: www.elsevier.com/locate/est

Carbon nanocomposite electrodes for electrical double layer capacitor

Allan Daraghmeh[a,b,*], Shahzad Hussain[b,c,*], Atta Ul Haq[c], Iyad Saadeddin[a], Llorenç Servera[d], JM Ruiz[d]

[a] Department of Physics, An-Najah National University, P.O. Box 7,Nablus, West Bank, Palestine
[b] Institute of Nanoscience and Nanotechnology (IN2UB), Universitat de Barcelona, Joan XXIII S/N, 08028, Barcelona, Spain
[c] Nanotechnology& Integrated Bio-Engineering Centre (NIBEC), Ulster University, Shore Road, Newtownabbey BT37 0QB, United Kingdom
[d] EscolaUniversitària Salesiana de Sarrià (EUSS), Passeig Sant Joan Bosco,74, 08217 Barcelona Spain

ARTICLE INFO

Keywords:
Nanocomposite
Carbon nanofibers
Activated carbon
Aqueous electrolyte
Electric double layer capacitor

ABSTRACT

Activated carbons (ACs) have been used as electrode material in commercial electric double-layer capacitors (EDLC) due to their low cost, high specific surface area, and chemical stability. Unfortunately, the super-capacitive performance of AC is not satisfactory due to their low conductivity.On the other hand, carbon nanofibers (CNFs) based EDLC exhibit low equivalent series resistance (*ESR*) but not such energy storage values as AC ones. Here in this paper, we report on the synthesis of new nanocomposites based on a mixture of ACs and CNFs using a simple powder processing route and evaluating their electrochemical behavior as electrode materials in symmetric EDLC. The EDLC, with 10 wt. % CNFs in AC/CNFs as the electrodes have displayed a high conductivity and surface area resulting in the enhancement of the energy and power delivers in aqueous electrolyte.

On the contrary, with 90 wt.% CNFs in AC/CNFs as the electrodes, higher specific power, low *ESR*, and low value of relaxation time constant are achieved. The highest value of specific capacitance estimated is around 207 F g^{-1} at 5 mV s^{-1} and the highest specific energy is 13.2 Wh kg^{-1} at 1 A g^{-1} for the 10 wt.% CNFs in AC/CNFs.

1. Introduction

Electrical double-layer capacitors (EDLCs) or supercapacitors are the emerging energy devices that possess high power densities. For applications demanding high power densities, the supercapacitors can be highly desirable and can also be used along with batteries for satisfying the needs of power density. For instance, in an electric vehicle, the power, and energy requirements can be achieved by supercapacitors and batteries, respectively [1]. The main shortcoming of the supercapacitors is low energy density.

The type and design of the electrode material are highly crucial in enhancing the electrochemical performance of the supercapacitors. Three types of electrode materials have mainly been utilized, namely activated carbons (ACs) [2–4], conjugated polymers [5], and some metal oxides [6]. Although the electrodes of metal oxides and conjugated polymers in supercapacitor enhance the energy densities, yet each electrode type has its limitations. For instance, most of the metal oxides have high costs and show weak reversibility during charge/discharge cycling that limits their commercial application. Similarly, instabilities are commonly attributed to electroactive polymers [7,8]. Carbon materials are widely used as supercapacitor electrodes. The compelling reason to use them in supercapacitors is due to their high surface area, low cost, and excellent chemical stability. The porous carbon electrodes of ACs [9], carbon nanofibers (CNFs) [10], graphene [11], and carbon nanotubes (CNTs) [12] have been used as supercapacitor electrodes to store large amounts of charges on their high surface areas. Mainly, the ACs are the commercially available materials used in supercapacitors with energy densities and power densities laying in the range of (8 Wh kg^{-1} and 825 W kg^{-1}) in acetonitrile electrolyte [13]. Due to their low electrical conductivity, their performance in supercapacitors is not satisfactory. Carbon nanofibers offer excellent electrical conductivity that can be accommodated in a supercapacitor electrode for current collection [14].

Nanocomposite electrodes based on carbon nanomaterials present an innovative electrode design for enhancing their supercapacitive properties. Susantyoko *et al.* prepared MWCNTs/AC based electrodes by a tape-casting procedure that delivered specific capacitance of 135.17 F g^{-1} at 1 A g^{-1} in 6 M KOH electrolyte [15]. Zhou *et al.* reported that the branched CNTs/CNFs composite delivers capacitance of 207 F g^{-1} at 1 A g^{-1} current density in H_2SO_4 electrolyte [16]. Zhou *et al.*

* Corresponding authors.
E-mail addresses: allan.d@najah.edu (A. Daraghmeh), s.hussain@ulster.ac.uk (S. Hussain).

https://doi.org/10.1016/j.est.2020.101798
Received 15 June 2020; Received in revised form 3 August 2020; Accepted 17 August 2020

synthesized a hybrid electrode of carbon nanotubes and graphitic nanofibers by a CVD method. The hybrid electrode presented 270 F g^{-1} capacitance at 1 A g^{-1} current density in 6 M KOH electrolyte [17]. Zhao *et al.* showed that CVD prepared graphene/single-walled CNTs deliver 98 F g^{-1} capacitance at 10 mV s^{-1} scan rate in 6 M KOH solution [18]. Luo *et al.* manufactured composite electrode based on carbon nanofiber/graphene nanosheet that displayed 215 F g^{-1} capacitance at 1 A g^{-1} in H_2SO_4 electrolyte [19]. Li *et al.* showed that the nitrogen-doped AC/reduced graphene oxide composite delivers 265 F g^{-1} capacitance at 50 mA g^{-1} current density in 7 M KOH electrolyte solution [20]. Xu *et al.* prepared CNTs/AC composited and tested in 6 M KOH aqueous electrolyte. The electrode showed a capacity of 267.6 F g^{-1} at a scan rate of 200 mV s^{-1} [21]. In other work, Pico F. *et al.* reported that cell resistance and capacitance decrease as the SWCNT contents increases according to the percolation model and rule of mixture [22].

In our previous work, the specific capacitance of AC and CNF electrodes were found to be around 334 F g^{-1} and 52 F g^{-1} at 5 mV $s^{-1,}$ respectively [23]. Furthermore, the internal resistances for the AC electrode and CNFs were 3.7 Ω and 0.2 Ω, respectively [23]. It was found that the CNFs supercapacitor showed low *ESR* values due to their high conductivity but delivered small capacitance due to their limited surface area. However, the high surface area of AC provides high specific capacitance values but endure higher *ESR* due to its low conductivity. The higher specific capacitance and low *ESR* values are, hence, the critical factors to achieve higher energy and power densities values.

Herein, we report on the synthesis of AC/CNFs composites with varying contents of CNFs in the composite using the powder processing method. Symmetric supercapacitor in aqueous solution resulted in excellent supercapacitive performance for 10 wt% CNFs in AC/CNFs. It was found that the specific capacitance was enhanced by decreasing the contents of the CNFs in the AC/CNFs composites. Furthermore, superior cyclability and high capacitive retention were achieved for our AC/CNFs composites than the ACs and CNFs alone.

2. Experimental section

2.1. Fabrication of AC/CNFs mixture electrodes

The carbon-based nanocomposite electrodes were fabricated by using the slurry method. The commercially available AC and CNFs were purchased from Donau Carbon supplied by Quimics Dalmau (reference Carbopal CCP80) and Grupo Antolin (GANF),respectively, with helicoidally graphitic stacked cup structure containing Ni (6 %). The diameter of the nanofibers was 20–80 nm in length and electric resistivity of 10^{-2} Ω•cm. The electrode preparation for supercapacitor was achieved by milling of AC/CNFs in an agate ball mill employing a frequency of 500 rpm for 30 min. The AC and CNFs were mixed using 15 ml of PVDF in acetone solution as a binder in an agate mortar. The slurry was then ultrasonicated for 30 min, followed by drying in a vacuum oven at 70 °C. The disc type electrodes of AC/CNFs were formed by pressing the AC/CNFs powder through a hydraulic press with a 10 mm die set to create the disc electrodes. The concentration of the CNFs in the composite electrodes was varied keeping the concentration of the PVDF constant at around 7 %, as summarized in Table 1. The mass and thickness of each electrode discs of AC/CNFs composite were around 20 mg and 0.38 mm respectively.

2.2. Materials characterization

The morphology of AC/CNFs nanocomposites was examined by scanning electron microscopy (SEM, Jeol J-7100) and transmission electron microscopy (TEM, Philips JEOL 2011) system operated at 300 kV. The porous texture and specific surface area of the AC/CNFs composites were obtained by physical adsorption of N_2 gas at 77 K using Micromeritics TriStar 3000 V6.04 A. All the samples were outgassed at 100 °C for 4 h before the adsorption measurements.

Table 1
Compositions of the activated carbons/carbon nanofibers (ACs/CNFs) nanocomposites prepared by the powder processing method.

Sample	CNFs weight percentage (%)
M1	10
M2	30
M3	50
M4	70
M5	90

The specific surface area (S_{BET}, m^2 g^{-1}) was calculated by multipoint Brunauer-Emmett-Teller (BET) procedure in the region of the isotherm, which is limited by the range of relative pressure (i.e. P/P_0 = 0.02–0.2). The total volume of pores (V_{total}, cm^3 g^{-1}) was then determined by the adsorbed N_2 quantity at $P/P_0 \approx 0.9932$. The volume of micropores and the values of surface areas were examined using the t-Plot Harkins and Jura method. The pore size distribution for all samples was calculated from adsorption isotherms obtained by the Barrett – Joyner – Halenda (BJH) and MP approach [23]. The *t*-plot Harkins and Jura methods were adopted to investigate the volume of micropores and the values of the BET surface area. The BJH adsorption cumulative pore volume was used to examine the meso and macro volume. The pore size distribution was then calculated from adsorption isotherms by using MP method for micropores and BJH method for meso and macropores.

The electrochemical performance of AC/CNFs composite electrodes in symmetric supercapacitor was investigated using a two-electrode Swagelok cell system with 6 M KOH solution as an electrolyte. The glass microfiber filter (MFV5) was used as a separator.

3. Results and discussion

3.1. Morphology of composite electrodes

Fig. 1(a) and (b) show the morphology of AC/CNFs composites containing 10 wt.% (M1) and 90 wt.% (M5) CNFs, respectively. It is evident that M1 consists of mainly ACs with few CNFs as compared to M5. The typical cylindrical and spherical shape of CNFs and ACs can be seen in Fig. 1(c) respectively. Fig. 1(c) represents the TEM images of the AC particles, which are found to be linked with the CNFs. The diameter of the ACs and CNFs, as estimated from TEM, was found to be around 100 nm and 85 nm respectively.

Fig. 2(a) displays the isotherms of AC/CNFs composites that reveal the maximum nitrogen adsorption that appears at a relatively low pressure (P/P_o < 0.02). The hysteresis loops become larger with the increase in CNFs concentration from 10 wt.% (M1) to 90 wt.% (M5) within the range of 0.45 to 0.8. This indicates varied porous structures of the samples as the concentration of CNFs are increased in the AC/CNFs composites.

By following the IUPAC classification [24], the isotherms of our samples lie in different regions (I, II, IV). The isotherm of sample M1 confirms their highly microporous nature. It hence can be classified as type I. The isotherms of samples M2-M4 exhibit a hysteresis loop in the middle to higher pressure range which classify them as multi type (I, II and IV) due to micro, meso and macropores respectively. However, the hysteresis loop of M5 classifies it into type (II and IV) as a result of meso and macropores respectively.

The specific surface area is calculated by multi-point BET technique in the range of 0–0.2, as shown in Fig. 2(b). In the previous study, we found that the specific areas for AC and CNFs were 1042 and 83 m^2 g^{-1}, respectively [23]. In the current work, the specific surface area of samples M1-M5 are around 939 m^2 g^{-1}, 640 m^2 g^{-1}, 482 m^2 g^{-1},

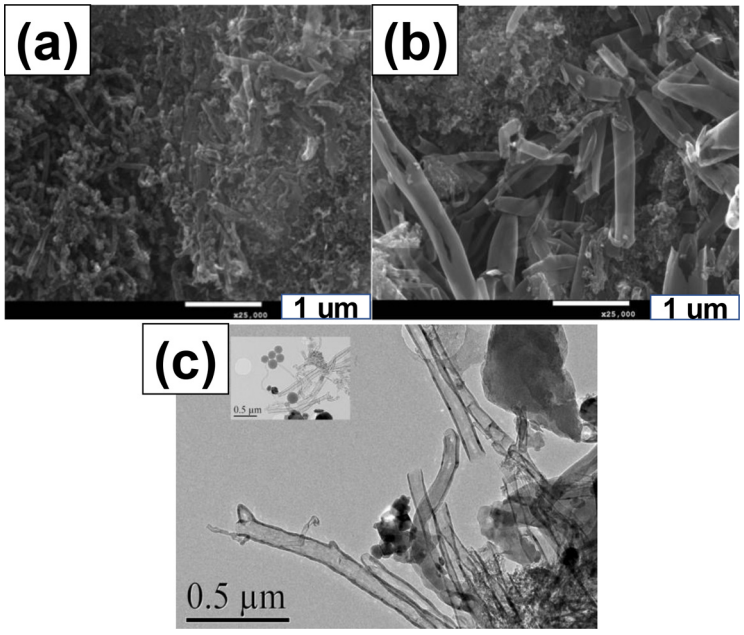

Fig. 1. (a-b) Scanning electron microscopy images of activated carbons - carbon nanofibers (ACs/CNFs) composite with 10 wt.% and 90 wt.% loading of CNFs respectively; **(c)** Transmission electron micrograph of AC/CNFs composite containing 10 wt.% CNFs.

404 $m^2\ g^{-1}$, and 184 $m^2\ g^{-1}$ respectively (see Table S1 in the Supplementary Information, SI). Hence, the higher contents of CNFs in AC/CNFs composite reduce the specific surface area of the nanocomposite.

Generally, the porous structures of nanomaterials are divided into three main groups i.e. (micro, meso and macro) pores for (<2 nm, 2–50 nm and >50 nm) respectively [24,25]. Fig. 2(c-d) represents the pore size distribution (PSD) obtained from the MP and BJH methods. The PSD in M1-M3, as derived from MP method, is shown in Fig. 2(c)

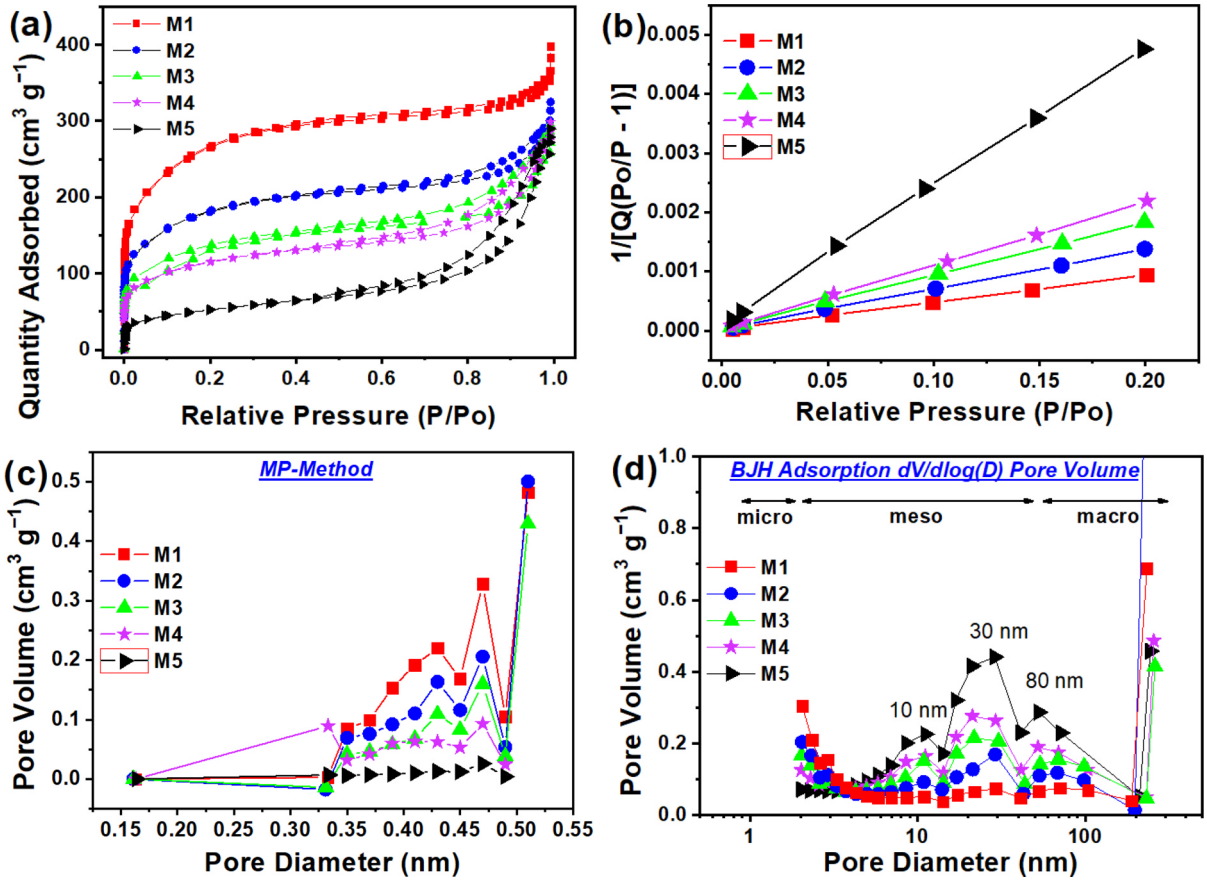

Fig. 2. (a) Nitrogen adsorption/desorption isotherms of ACs/CNFs composite containing 10 wt.% (M1), 30 wt.% (M2), 50 wt.% (M3), 70 wt.% (M4) and 90 wt.% (M5) CNFs respectively. **(b)** the surface areas of ACs/CNFs estimated by the Branauer-Emmet-Teller (BET) method; **(c-d)** the pore sizes of ACs/CNFs deduced from Micropore analysis (MP) and Barret-Joyner-Helenda (BJH) methods respectively.

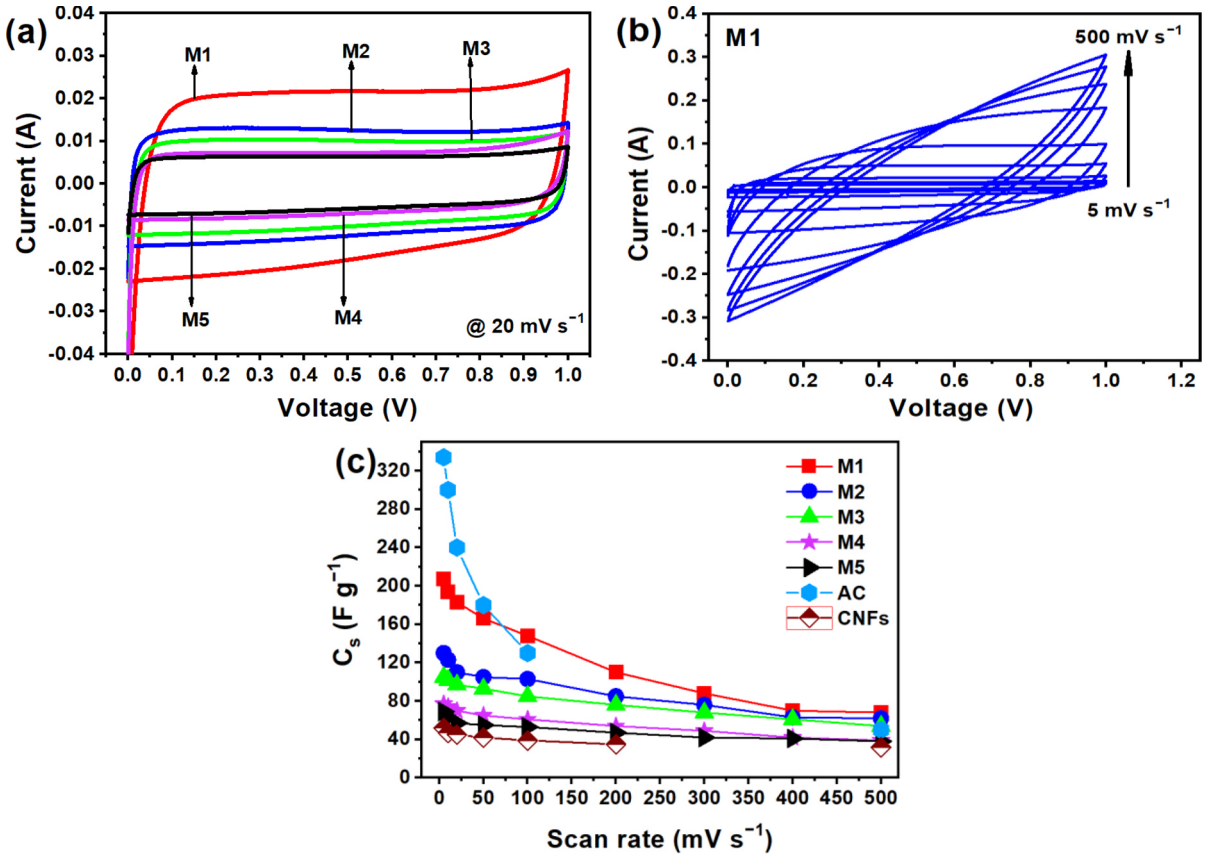

Fig. 3. (a) Cyclic voltammograms (CVs) of activated carbons/carbon nanofibers (ACs/CNFs) composites at a scan rate of 20 mV s^{-1}; **(b)**CVs of AC/CNFs containing 10 wt.% CNFs (M1) from 5 mV s^{-1} to 500 mV s^{-1}; **(c)** the changes in the specific capacitance of AC-CNFs, ACs and CNFs with increasing the scan rates from 5 mV s^{-1} to 500 mV s^{-1}. The C_s values of AC and CNFs are taken from a previous study [23].

and suggests that the dominant porous structure mainly lie in the range of 0.4–0.5 nm. While M4 and M5 samples show a tiny number of micro pores within the same range. The PSD from the BJH method Fig. 2(d) indicates the existence of main pores about size of 2 nm for both M1 and M2; and 10 nm, 30 nm and 70 nm for M3–M5.

3.2. Electrochemical performance of composite electrodes in symmetric supercapacitor

The specific capacitance values, calculated from CVs, by using the equations (1) and (2) in the Supplementary Information (SI), are shown in Fig. 3. The Fig. 3(a) presents the comparison of the CVs of M1–M5 samples at a scan rate of 20 mV s^{-1}. All samples showed highly rectangular-shaped CVs, confirming the typical behaviour of EDLCs. Furthermore, the integrated area of the CVs follows the sequence M1 > M2 > M3 > M4 > M5. It can be concluded that the M1 accumulates the highest number of charges in comparison to other samples at a similar scan rate. The Fig. 3(b) shows the CVs of M1 at scan rates from 5–500 mV s^{-1}. The rectangular nature of the CVs indicates that the supercapacitive behaviour is entirely based on the electrostatic mechanism. The CVs at 5–500 mV s^{-1} scan rates for M2, M3, M4 and M5 are also shown in SI (Fig. S1).

Fig. 3(c) shows the shifts in the specific capacitance (C_s) with the change in the scan rates of samples (M1–M5). It is a well-known fact that the C_s values are higher at low scan rates because the enough time is available for the ions to reach at accessible pores of the electrode and form the EDL [26], and with the increase of the scan rate the $C_s$decreases monotonously. Interestingly, the decrease in the C_s of ACs is found to be much drastic than the AC/CNFs mixture. With the increase in scan rate from 5 mV s^{-1} to 100 mV s^{-1}, the C_s was found to be decreased by 61% for AC, while the same dropped by only 28.5% and 25% for M1 and CNFs respectively. Furthermore, a careful comparison of CV spectra obtained for ACs, M1 and CNFs, at different scan rates, revealed that at low scan rate (10 mV s^{-1}) all the supercapacitors show a rectangular shape CV profile as shown in Fig. S2a. However, as observed from Fig. S2b, at higher scan rate (100 mV s^{-1}) the CV scan became more sensitive revealing the superiority of the CFs or AC/CFs composites-based electrodes. Thanks to high electrical conductivity of CNFs, CNFs and M1 supercapacitors keep the rectangular shape even at higher scan rate, which imply ideal capacitor behaviour. However, due to poor electrical conductivity of AC, its CV shape change from rectangular to diamond like, which is indicative of poor rate performance [21,27]. As the scan rate reached 100 mV s^{-1} the M1 supercapacitor starts to deliver higher specific capacitance than AC supercapacitor. This can be due to higher electric conductivity of nanocomposite M1 which makes the electron transportation easier during CV scans. The C_s of M1 and M5 supercapacitors were found to be around 207 F g^{-1} and 69 F g$^{-1,}$ respectively at a scan rate of 5 mV s^{-1}. The M1 supercapacitor, hence, displays the highest C_s value, as shown in Fig. 3(c) compared to M2–M5 supercapacitors. The highest C_s values of M1 are due to contributions from both the high surface area provided by AC and good electrical conductivity contributed by CNFs in the composite. Furthermore, the overall behaviour of the C_s in AC/CNFs is far better than the ACs and CNFs alone as shown in Fig. 3(c).

Fig. 4(a) presents the comparison of galvanostatic charge-discharge (GCD) curves of our supercapacitors M1–M5 measured at a current density of 1 A g^{-1}. The almost symmetrical shape of the charge-discharge cycles of M1–M5 is the indication of the high electrochemical reversibility of supercapacitors. These types of curves are like those exhibited by carbon-based supercapacitors. The charge-discharge times

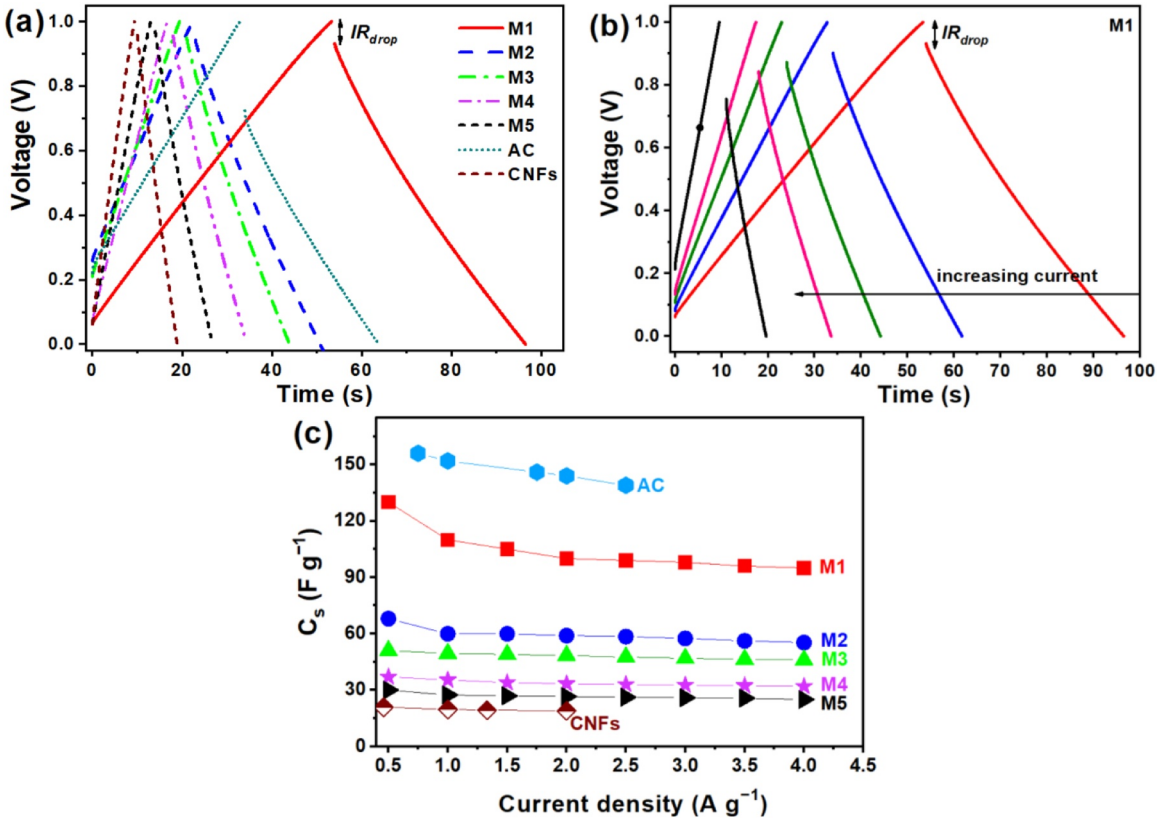

Fig. 4. (a) The charge-discharge curves of activated carbons/carbon nanofibers (AC-CNFs) symmetric supercapacitors measured at a current density of 1 A g^{-1}; **(b)** charge-discharge cycles of ACs/CNFs with 10 wt.% (M1) CNFs at the current densities of 1, 1.5, 2, 2.5 and 4 A g^{-1}; **(c)** curves of specific capacitances versus scan rates of AC/CNFs composite electrodes in the symmetric supercapacitors with compositions of 10 wt.%, 30 wt.%, 50 wt.% 70 wt.% and 90 wt.% CNFs labelled as M1-M5, respectively. The charge-discharge curves and specific capacitances values of AC and CNFs are taken from a previous study [23].

in M1 supercapacitor is larger than the rest of the supercapacitors (i.e. M2–M5) which indicates that a higher number of electrons and electrolyte ions are shared in charge-discharge processes. Fig. 4(b) shows GCD curves at current densities from 1 A g^{-1} to 4 A g^{-1} for the M1 supercapacitor. The charge and discharge curves are nearly symmetrical in shape, with varying potential drops (IR_{drop}) at the reversal of the current. The small IR_{drop} at low current tells the low value of equivalent series resistance (*ESR*).

The *ESR* values from charge-discharge curves calculated, using equation (3) in SI, at 1 A g^{-1} were found to be around 0.034 Ω, 0.029 Ω, 0.025 Ω, 0.022 Ω and 0.015 Ω for the M1–M5 supercapacitors respectively. The higher *ESR* in M1 is due to the low quantity of CNFs in the AC/CNFs composite in comparison to others. This confirms that an increase in the CNFs concentration of these samples causes a decrease in the *ESR* values, which is due to the conductivity of the CNFs. In previous study we found the *ESR* values for AC and CNFs were 0.138 Ω and 0.01 Ω respectively [23].

The discharge capacitance from the GCD curve is estimated by applying equation (4) in SI. Fig. 4(c) presents a comparison of the variation on the C_s values, determined from the GCD curves, with changing the current densities for M1–M5 supercapacitors. The M1 supercapacitor exhibits a high C_s value ~130 F g^{-1} at a current density of 0.5 A g^{-1} and low C_s value ~95 F g^{-1} at a current density of 4 A g^{-1}. The decrease in C_s with an increase in current density is very common for supercapacitors and is mainly originated by the diffusion limitation of the electrolyte ions inside the micropores of the electrode. A similar behaviour of decrease in the C_s with an increase in current density from 0.5 A g^{-1} to 4 A g^{-1} was observed for M2-M5 supercapacitors as shown in Fig. 4(c). It is remarkable that the C_s in M1 supercapacitor is almost five-times higher than the value of the specific capacitance for M5.

Fig. 5(a), shows the Ragone plot of our supercapacitors. The specific energy and specific power (see equations (5) and (6), in SI, respectively) of M1-–M5 electrodes at 1 A g^{-1}, which are compared with the ACs and CNFs results. It is evident that the addition of 10 wt.% CNFs in AC changes their specific energy from 11 Wh kg^{-1} to 13.26 Wh kg^{-1} and specific power from 1331 W kg^{-1} to 1126 W kg^{-1} at the same current density of 1 A g^{-1} from ACs to M1 supercapacitors.These findings indicate excellent electrochemical characteristics for the supercapacitors of AC/CNFs composite electrodes with high energy and power output. Therefore, these supercapacitors can prove to be very attractive for those applications where high power and energy are demanded [28]. Fig. 5(b) shows the cyclic stability of samples up to 8000 charge discharge cycles at a current density of 1.5 A g^{-1}. All samples show high stability in capacitance with a capacity retention of around 96% for M1, 91% for M2, 94% for M3, 94% for M4, and 97% for M5.

Further, all samples were characterized by electrochemical impedance spectroscopy (EIS), and their corresponding data are presented as the Nyquist plot in Fig. 6(a). The starting impedance value measured at the highest frequency (at 100 kHz) represents the electrolyte solution resistance [29,30], R_{soln}, which was found to be around 0.16 Ω, same for all the supercapacitor cells. However, the arc resistance (R_{arc}), visualized by the high to mid-frequency semicircles in the Nyquist plots (Fig. 6a), attributing to the combined resistance of the nanocomposites and the composite/collector contacts, depends on the concentrations of the nanomaterials (ACs, CNFs). The resistance R_{arc}values were estimated to 0.93, 0.84, 0.61, 0.43 and 0.37 Ω for M1, M2, M3, M4, and M5 respectively. The R_{arc}value decreased with an increase in the concentration of CNFs in the composites because of the higher conductivity of the CNFs. The R_{arc}value for M1 is 0.93 Ω which is significantly lower than 3.56 Ω for the AC electrodes only as reported in our previous paper [23]. Hence, the addition of a small number of CNFs in AC supports the decrease in the R_{arc}value of the electrode. The total resistance *ESR*,

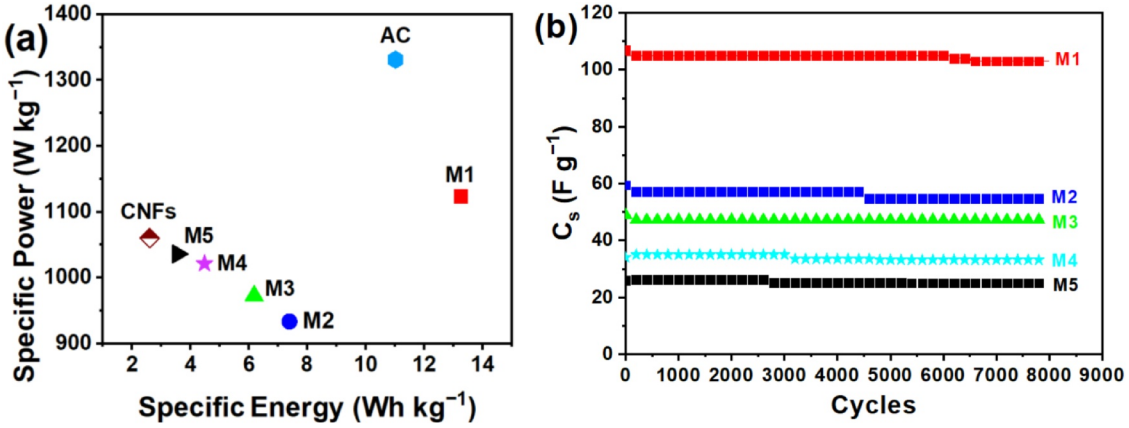

Fig. 5. (a) Ragone plot comparison at 1 A g^{-1} current density,the values of AC and CNFs are taken from a previous study [23]; **(b)** long term cyclic stability measured at a current density of 1.5 A g^{-1}.

combining $R_{arc}$and R_{soln} values, is 1.09, 1, 0.77, 0.59, and 0.53 Ω for samples M1, M2, M3, M4, and M5 respectively. The *ESR* values decreased as well with an increase in CNFs concentrations. Low *ESR* values make these composite materials very promising for the application under study [29].

Furthermore, two important parameters namely knee frequency and relaxation time constant τ_0 were evaluated to determine the performance of the supercapacitors, as shown in Fig. 6(b, c). The knee frequency appears at phase angle 45° identifies the resistive and capacitive portions of the supercapacitor. The knee frequency appears at 0.08, 0.2, 0.3, 0.8, and 0.98 Hz for sample M1, M2, M3, M4, and M5 respectively. The relaxation time constant τ_0 divides the resistive and capacitive parts of the supercapacitor. The low values of τ_0 are desirable to have power transfer. The plot Fig. 6(b, c), imaginary capacitance vs frequency (f) is adopted to find the value of τ_0. The imaginary capacitance (C'') is calculated by using equation (7) in SI. The reciprocal of frequency where the maximum is obtained is called the time constant ($\tau_0 = 1/f_0$). This gives relaxation time constant τ_0 of 12.5 s, 5 s, 3.3 s, 1.2 s, and 1.0 s for M1, M2, M3, M4, and M5 respectively. These results show that τ_0 decreases with the increase in the concentration of CNFs.

The C_s values of the supercapacitor at different frequencies were also calculated by the imaginary component of the impedance (by using equation (8) in SI. The C_s, estimated from the impedance measurements, were found to be around 201 F g^{-1}, 114 F g^{-1}, 100 F g^{-1}, 64 F g^{-1} and 50 F g^{-1} for M1- M5 supercapacitors respectively, as shown in Fig. 6(d). At high frequencies, the low C_s values are delivered because supercapacitors start working as resistors at high frequencies. Furthermore, it is interesting to note here that the C_s obtained from EIS is

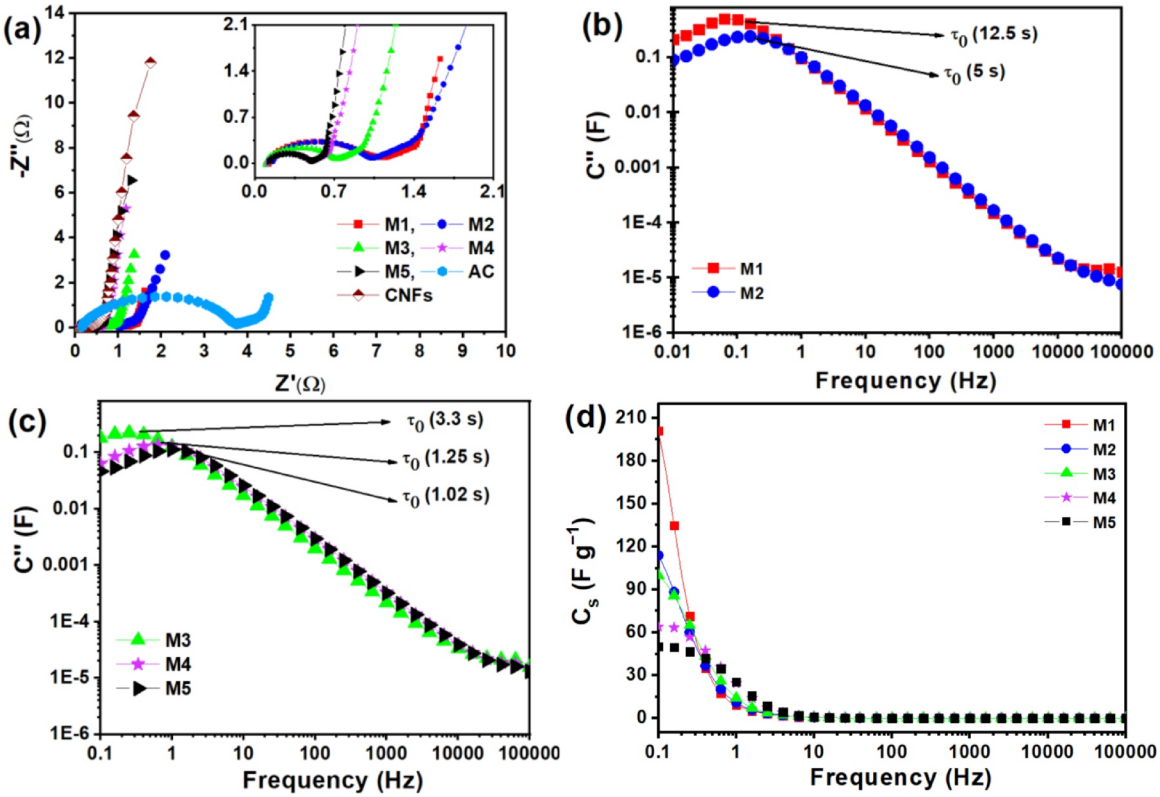

Fig. 6. (a) Nyquist plots of activated carbons (ACs), carbon nanofibers (CNFs), ACs/CNFs composites with 10 wt.% (M1), 30 wt.% (M2), 50 wt.% (M3), 70 wt.% (M4), and 90 wt.% (M5) CNFs;**(b-c)** The imaginary capacitance (C″)as a function of frequency; **(d)** variation in the capacitance as a function of frequency. The Nyquist plot values of AC and CNFs are taken from a previous study [23].

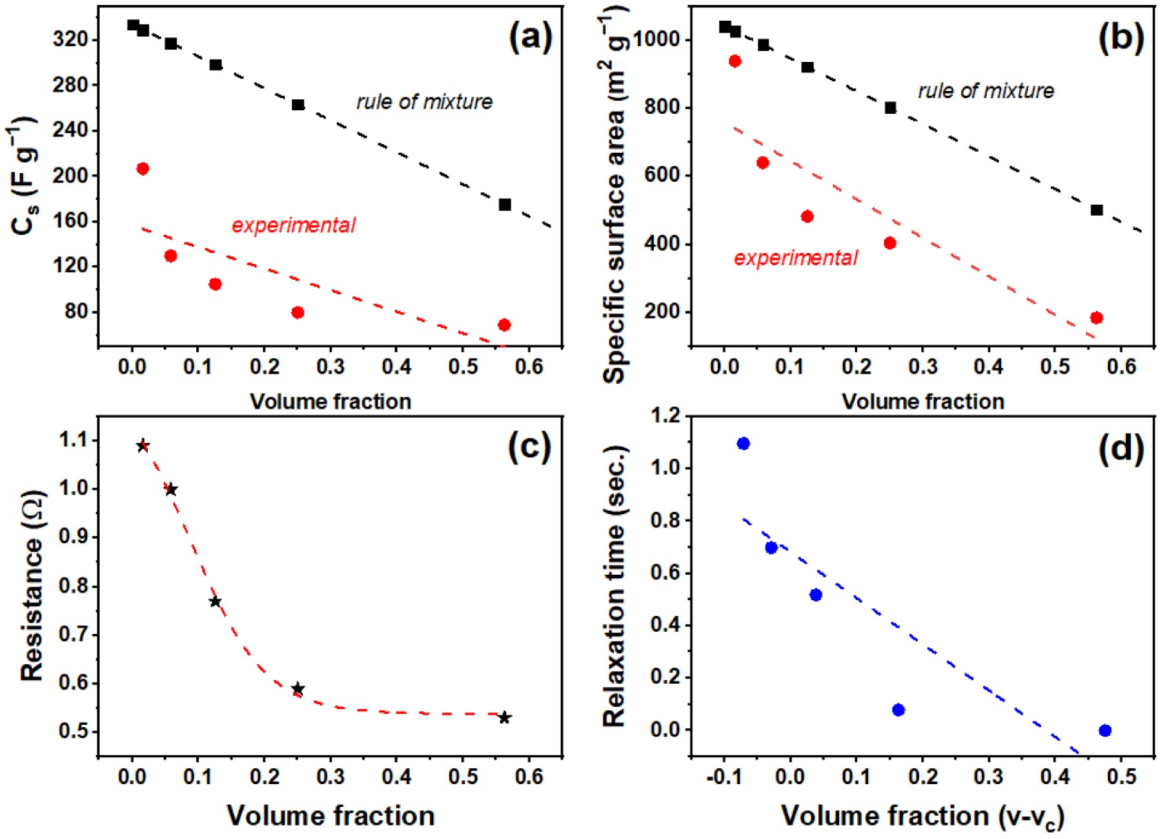

Fig. 7. (**a-b**) The changes in the specific capacitance and specific surface area versus the volume fraction of carbon nanofibers are compared with the rule of mixtures, respectively. The specific capacitance is estimated from the cyclic voltammograms at a scan rate of 5 mVs^{-1}. The dashed lines represent the linear fit; (**c**) The s-curve of resistance versus volume fraction following the percolation model (sigmoidal-Boltzmann). The percolation threshold (v_c) is 0.087 as deduced from the fit line; (**d**) The changes in the relaxation time versus the volume fraction as plotted in logarithmic scale.

very close to that calculated from CV measurements.

Fig. 7a shows the specific capacitance of the composites (M1–M5), obtained from CV, versus the volume fractions of CNFs (as calculated using the relation given in this paper [31], which are also compared with the data deduced by applying the rule of mixtures to the composite. The changes in the specific capacitance follows nearly a linear trend much like the rule of mixtures trend line. Similar trend has been observed for the changes in the specific surface area with the changes in the volume fraction as shown in Fig. 7b.

For the percolation of CNFs in the AC matrix, we have plotted the electrode resistance versus the volume fraction curve which resembles nearly a S-shaped curve following the sigmoidal-Boltzmann behaviour [22,31,32]. The threshold value of CNFs, at which the percolation network is formed, is found to be around 0.087 which is extracted from the fit line of the curve in Fig. 6c. This is the content of CNFs at which the resistance of the composite sharply decreases and follows the saturation at higher concentrations of CNFs. Such threshold value of the filler material depends on the conductivity and aspect ratio of the filler material. The conductivity and aspect ratio of CNFs are lower than CNTs, hence the percolation threshold is higher than the composites containing CNTs as a filler material [22]. The percolation threshold in composites is related to the aggregation and the high aspect ratio of CNFs. Lastly, the delivery of power in supercapacitor is affected by the relaxation times. The changes in the relaxation times in our supercapacitors, as discussed earlier, versus the volume fraction of CNFs are plotted in Fig. 7d. The fit line of the plot resulted in the negative slope of 7.6 s which is quite low in case of AC/CNFs composites.

4. Conclusions

We have successfully prepared current collector free supercapacitors with different contents of AC and CNFs. The high contents of AC, i.e. low amounts of CNFs, in the AC/CNFs composites, provide mainly micro and ultramicroporous structure, resulting in a specific surface area of 939 m^2 g^{-1}. In contrast, the sample with higher CNFs loading consists of mainly mesopores with a low specific surface area of around 184 m^2 g^{-1}. The higher specific capacitance of 207 F g^{-1} at 5 mV s^{-1} for M1 is due to their high specific surface area, low external surface area and shorter diffusion length of ions. The resistance values for the Rarc are less than 1 Ω for all samples. The small amount of CNFs addition to AC makes a strong network between AC particles and, hence, increases the conductivity of the electrodes. The relaxation time constant values determined by EIS and are in the range of 1 to 12.5 s for M5 to M1, respectively. The highest specific energy of 13.26 Wh kg^{-1} and specific power of 1126 W kg^{-1} wereattainable at 1 A g^{-1}, indicating superior energy storage characteristics. The charge/discharge cycling stability was studied up to 8000 cycles and presents higher stability in capacitance at 1.5 A g^{-1} current density. The superior energy storage capability of carbon nanocomposite (AC/CNFs) electrode in an aqueous electrolyte made them promising materials for high energy and high-power applications.

Declaration of Competing Interest

None.

Acknowledgments

A. Daraghmeh acknowledges the Centre d'Enginyeria de Micro iNanosistemes per InstrumentacióiComunicacions (CEMIC-UB), and Escola UniversitariaSalesiana de Sarria (EUSS) for supplying CNF, GO and rGO samples.

Supplementary materials

Supplementary material associated with this article can be found, in the online version, at doi:10.1016/j.est.2020.101798.

References

[1] P. Simon, Y. Gogotsi, B. Dunn, Where do batteries end and supercapacitors begin? Science 343 (6176) (2014) 1210–1211.
[2] B.E. Conway, Electrochemical Supercapacitors, Scientific Fundamentals and Technological Applications, Kluwer Academic/Plenum Publishers, New York, 1999, pp. 11–31.
[3] E. Raymundo-Piñero, K. Kierzek, J. Machnikowski, F. Béguin, Relationship between the nanoporous texture of activated carbons and their capacitance properties in different electrolytes, Carbon 44 (2006) 2498–2507.
[4] M. Inagaki, H. Konno, O. Tanaike, Carbon materials for electrochemical capacitors, J. Power Sources 195 (2010) 7880–7903.
[5] M. Wu, Q. Zha, J. Qiu, Y. Guo, H. Shang, A. Yuan, Preparation and characterization of porous carbons from PAN-based preoxidized cloth by KOH activation, Carbon42 (2004) 205–210.
[6] M. Kazazi, M. Faryabi, Electrochemically anchored manganese hexacyanoferrate nanocubes on three-dimensional porous graphene scaffold: towards a potential application in high-performance asymmetric supercapacitors, J. Power Sources 449 (2020) 227510.
[7] N. An, Y. An, Z. Hu, Y. Zhang, Y. Yang, Z. Lei, Green and all-carbon asymmetric supercapacitor based on polyaniline nanotubes and anthraquinone functionalized porous nitrogen-doped carbon nanotubes with high energy storage performance, RSC Adv. 5 (2015) 63624–63633.
[8] I. Shown, A. Ganguly, L-C Chen, K-H Chen, Conducting polymer-based flexible supercapacitor, Energy Sci. Eng.3 (2015) 2–26.
[9] T. Sesuk, P. Tammawat, P. Jivaganont, K. Somton, P. Limthongkul, W. Kobsiriphat, Activated carbon derived from coconut coir pith as high performance super-capacitor electrode material, J. Energy Storage 25 (2019) 100910.
[10] E. Stojanovska, A. Kilic, Carbon nanofibers as thick electrodes for aqueous super-capacitors, J. Energy Storage 26 (2019) 100981.
[11] M.-H. Phama, A. Khazaelia, G. Godbille-Cardonaa, F. Truica-Marasescub, B. Peppleya, D.P.J. Barza, Printing of graphene supercapacitors with enhanced capacitances induced by a leavening agent, J. Energy Storage 28 (2020) 101210.
[12] S. Hussain, E. Kovacevic, R. Amade, J. Berndt, C. Pattyn, A. Dias, C. Boulmer-Leborgne, M.-R. Ammar, E. Bertran-Serra, Plasma synthesis of polyaniline enrobed carbon nanotubes for electrochemical applications, Electrochim. Acta 268 (2018) 218–225.
[13] A. Burke, R&D considerations for the performance and application of electro-chemical capacitors, Electrochim. Acta 53 (2007) 1083–1091.
[14] A.G. Pandolfo, A.F. Hollenkamp, Carbon properties and their role in supercapacitors, J. Power Sources 157 (2006) 11–27.
[15] R.A. Susantyoko, F. Parveen, I. Mustafa, S. Almheiri, MWCNT/activated-carbon freestanding sheets: a different approach to fabricate flexible electrodes for super-capacitors, Ionics25 (2019) 265–273.
[16] Y. Zhou, X. Zhou, C. Ge, W. Zhou, Y. Zhu, B. Xu, Branched carbon nanotube/carbon nanofiber composite for supercapacitor electrodes, Mater. Lett. 246 (2019) 174–177.
[17] Y. Zhou, P. Jin, Y.Z. YatongZhou, High-performance symmetric supercapacitors based on carbon nanotube/graphite nanofiber nanocomposites, Sci. Rep. 8 (2018) 9005.
[18] M.-Q. Zhao, Q. Zhang, J.-Q. Huang, G.-L. Tian, T.-C. Chen, W.-Z. Qian, F. Wei, Towards high purity graphene/single-walled carbon nanotube hybrids with im-proved electrochemical capacitive performance, Carbon54 (2013) 403–411.
[19] H. Luo, P. Xiong, J. Xie, Z. Yang, Y. Huang, J. Hu, Y. Wan, Y. Xu, Uniformly dis-persed freestanding carbon nanofiber/graphene electrodes made by a scalable biological method for high-performance flexible supercapacitors, Adv. Funct. Mater. 1803075 (2018) 1–9.
[20] Y. Li, T.-X. Shang, J.-M. Gao, X.-J. Jin, Nitrogen-doped activated carbon/graphene composites as high-performance supercapacitor electrodes, RSC Adv. 7 (2017) 19098–19105.
[21] G. Xu, C. Zheng, Q. Zhang, J. Huang, M. Zhao, X.W. JingqiNie, F. Wei, Binder-free activated carbon/carbon nanotube paper electrodes for use in supercapacitors, Nano Res. 4 (2011) 870–881.
[22] F Pico, C Pecharroman, A Ansón, Martinez M Teresa, JM Rojo, Understanding carbon-carbon composites as electrodes of supercapacitors, J. Electrochem. Soc. 154 (6) (2007) A579–A586.
[23] A. Daraghmeh, S. Hussain, I. Saadeddin, E.X. LlorençServera, A. Cornet, A. Cirera, A study of carbon nanofibers and active carbon as symmetric supercapacitor in aqu-eous electrolyte: a comparative study, Nanoscale Res. Lett. 12 (2017) 639.
[24] S J Gregg, K S W Sing, 2nd ed., Adsorption, Surface Area and Porosity 4 Academic Press, New York, 1982, p. 287.
[25] J. Huang, B.G. Sumpter, V. Meunier, A universal model for nanoporous carbon supercapacitors applicable to diverse pore regimes, Chemistry 14 (2008) 6614–6626.
[26] J. Yan, T. Wei, B. Shao, Z. Fan, W. Qian, M. Zhang, F. Wei, Preparation of a gra-phene nanosheet/polyaniline composite with high specific capacitance, Carbon48 (2010) 487–493.
[27] F. Cheng, X. Yang, S. Zhang, W. Lu, Boosting the supercapacitor performances of activated carbon withcarbon nanomaterials, J. Power Sources 450 (2020) 227678.
[28] M Endo, T Maeda, T Takeda, Y J Kim, K. Koshiba, H. Hara and, M.S. Dresselhaus, Capacitance and pore-size distribution in aqueous and nonaqueous electrolyte using various activated carbon electrodes, J. Electrochem. Soc. 148 (2001) A910–A924.
[29] H. Xia, Y. Wang, J. Lin, L. Lu, Hydrothermal synthesis of MnO_2/CNT nanocomposite with a CNT core/porous MnO_2 sheath hierarchy architecture for supercapacitors, Nanoscale Res. Lett. 7 (2012) 33.
[30] C.Y. Lee, H.M. Tsai, H.J. Chuang, S.Y. Li, P. Lin, T.Y. Tseng, Characteristics and electrochemical performance of supercapacitors with manganese oxide-carbon na-notube nanocomposite electrodes, J. Electrochem. Soc. 152 (2005) A716–A720.
[31] A.A. Vasileiou, M. Kontopoulou, A. Docoslis, A noncovalent compatibilization ap-proach to improve the filler dispersion and properties of polyethylene/graphene composites, ACS Appl. Mater. Interfaces 6 (3) (2014) 1916–1925.
[32] M. Rahaman, A. Aldalbahi, P. Govindasami, N.P. Khanam, S. Bhandari, P. Feng, T. Altalhi, A new insight in determining the percolation threshold of electrical conductivity for extrinsically conducting polymer composites through different sigmoidal models, Polymers 9 (10) (2017) 527.